JIT Mahasarakham University, Thailand
http://jit.it.msu.ac.th

Journal of Applied Informatics and Technology, 7(2), 305-324.

Research Article

Classification of Guanxi Mandarin Orange Grades using Machine Vision Algorithms

Fulian Huang[1], Jialin Xie[2], Shijun Jie[3], Nattawoot Suwannata[1,*]

[1] Faculty of Engineering, Mahasarakham University, Mahasarakham 44150, Thailand
[2] Faculty of Electrical and Electronic Engineering, Guilin University of Technology, Guilin, Guangxi 541000, China
[3] Faculty of Mechanical and Control Engineering, Guilin University of Technology, Guilin, Guangxi 541000, China
* Corresponding author: Nattawoot Suwannata, nattawoot.s@msu.ac.th

Received:
12 September 2024
Revised:
25 December 2024
Accepted:
26 March 2025

Keywords:

Classification, Defect, Detection, Flaw, Machine Vision System, Mandarin Orange, Skin

Abstract: This article proposes a method for categorizing Mandarin orange grades based on Chinese standards using a computer vision system that integrates both hardware and software components. A mechanical roller-flipping device adjusts the Mandarin orange's position in various orientations. Subsequently, a machine vision system acquires thirty photographs of mandarin orange skin from various viewpoints and employs many processing approaches, such as image acquisition, blob analysis, preprocessing, segmentation, and feature extraction. The process of classifying oranges involves applying techniques such as morphology, median filtering, and the Fourier transform to identify and analyze pixels that represent imperfections on the surface of the orange. Then the faulty pixels are transformed into the diameter and the area of the faults in order to classify them for grading. The experiment demonstrates that the diameter and rectangular regions can be utilized to categorize Mandarin oranges into three grades: Special Grade, Grade 1, and Grade 2. Grade 3 can be determined by measurement of the diameter and calculation of the percentage of the faulty region in the orange peel. The overall recognition accuracy by the system is 87.5%. This experimental method can accurately identify defects in the skin of oranges, reducing labor costs and the error rate of manual identification for enterprises.

1. Introduction

Citrus cultivation covers an area of 1.85 million mu (123,333 hectares) in Guangxi, China, yielding an output of 4.7 million tons. China is the foremost global producer of citrus fruits and maintains a substantial role as an exporter of oranges (Spreen *et al*., 2020). Nevertheless, the primary challenge is devising a method to differentiate ill or contaminated oranges from high-quality oranges, with the aim of maintaining quality control over mandarins throughout the whole process. The key types of diseases that impact citrus include oil spot disease, penicillium, scab disease, Mal secco disease, anthrax, melanin diseases, brown spot disease, phytophthora, and citrus ulcers (Garg *et al*., 2023; Batuman *et al*., 2020). This article primarily concentrates on the visual categorization and arrangement of orange skin resulting from melanosis and melanin synthesis.

Machine vision is currently a key technology in the field of intelligent devices and automation (Kamalakannan & Rajamanickam, 2012; Dey, Biswas, & Le, 2023; Sangkatip, 2024). In order to improve the efficiency of orange defect detection and to avoid the following shortcomings of manual inspection: 1) Inefficiency. 2) High error rate. 3) Impact on the well-being of inspectors. 4) Citrus is easily damaged (Huang *et al*., 2021). In this study, taking the skin characteristics of citrus as the research object, a hardware system consisting of an industrial camera (Hikvision Industrial Camera MV-CU013-21UM), a conveyor belt, and a computer was constructed, and the photographs captured by the industrial camera were transmitted to the computation, and the Halcon software was used to process the images for image processing, and according to the Chinese orange epidermal defects evaluation criteria, and finally output the grade of the detected oranges. Compared with the existing thesis design, the main innovation of this thesis is the use of hardware with rollers that can automatically flip Mandarin orange, and the camera automatically captures 30 photos of Mandarin orange with different sides for analysis. Through this method of detection, it can greatly save the labor cost and improve the detection efficiency.

2. Literature Review

In recent years, the advancement of machine vision research has led to a significant increase in its potential uses in agriculture. Chen, Wu, & Cui (2018) first applied preprocessing and segmentation on the orange photographs to extract their relevant features. Subsequently, they utilized neural networks to automatically classify orange grades. The classification strategy achieves an accuracy of 94.38%. Dharmasiri & Jayalal (2019) successfully detected passion fruit illness with an accuracy rate of 79% using the Support Vector Machine (SVM) algorithm. They also classified the disease environment into three categories: mild, moderate, or severe. Prabhu, Likhitha, & Sangeetha (2021) suggested a classification model that was 97% accurate after looking at how well KNN, SVM, and DT classifiers did

at putting oranges into groups. Dheeraj *et al*. (2023) utilized convolutional neural networks to analyze the imperfections in okra. They achieved an impressive accuracy of 98.63% for VGG-16. Hafiz & Fatema (2023) achieved a final accuracy of 96.17% in identifying wax apple disease by utilizing machine learning approaches to forecast preprocessed pictures. In the study, Mojumdar & Chakraborty (2021) got an overall classification accuracy of up to 82.3% by taking 13 features from segmented photos and using the gray scale co-occurrence matrix in image processing. Behera, Jena, Rath & Sethy (2018) utilized multi-class SVM and K-means clustering to classify citrus illnesses with 90% accuracy. These techniques, basically, require preprocessing the image before adding the algorithm for training. This design is analyzed based on the captured images and combines the image processing methods from the above literature to finalize the defect detection.

Until recently, machine vision technology has not employed many photographs of each fruit to identify defects in citrus or other crops. Hence, the analytical results do not cover the complete surface of the fruit. This article presents a technique for taking comprehensive photographs of whole oranges utilizing an automated rolling apparatus. Afterward, all pictures underwent image processing procedures to detect imperfections in the texture of the orange peel. The least desirable results from each shot were then compared to categorize the quality of the oranges based on Chinese criteria.

3. Methodology

3.1 Orange Grade Classification Standard

Currently, the orange industry and the Chinese government have established guidelines for the Mandarin orange classification. The national standard, GB/T 40752-2021 (2021), holds significant importance in this classification. Table 1 shows the spot diameter of the Mandarin orange according to the Chinese standard.

3.1 Machine Vision Inspection Systems

The techniques for detecting a flaw in Mandarin oranges are based on machine vision technology. Specific image processing algorithms are used to detect the size of the

Table 1. Defected spot diameter of Mandarin orange

Grade	Spot diameter
Special grade	No flower skin, no festering, no scars.
Grade 1	D > 0 - 1.6 mm
Grade 2	D > 1.6 – 7 mm.
Grade 3	D > 7 mm. Defect area > 10%

defect diameter from the industrial camera-captured pictures and then determine the grade of mandarin oranges according to Chinese standards. Figure 1 shows the Mandarin orange machine vision detection system's hardware. The process of automatic defect detection is as follows:

1) The conveyor system loads the Mandarin oranges onto the rollers upon activation. The light source automatically turns on. While the roller is rolling, the industrial camera captures pictures of each Mandarin orange from various angles, as shown in Figure 2.

2) The computer processes the images of 30 pictures from various angles for defect detection using image processing algorithms written by Halcon software.

3) The classification of orange grades is determined by comparing the diameter size of defects in pixels with the actual diameter in millimeters, as indicated in Table 1.

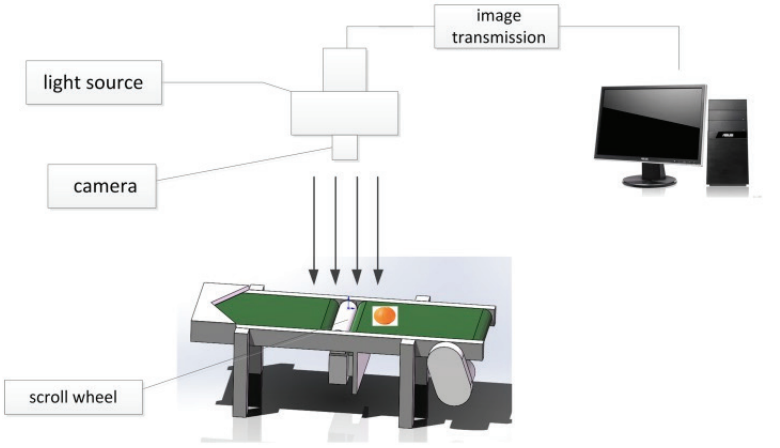

Figure 1. System for classifying orange grades

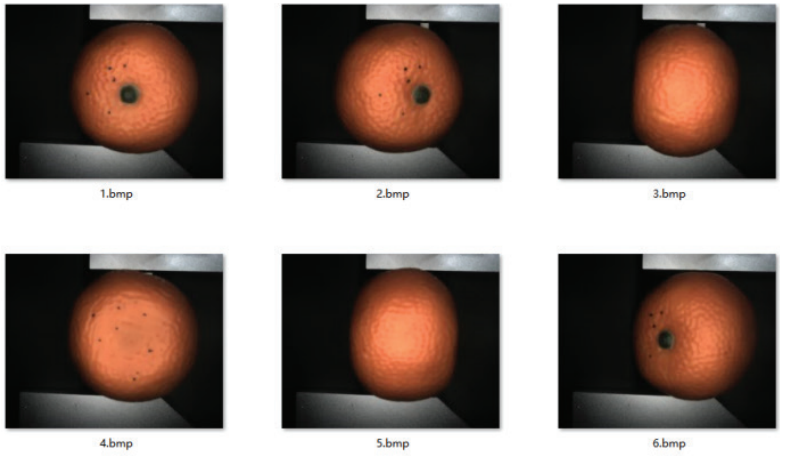

Figure 2. Photos taken by mandarin Orange under industrial cameras (6 representative images from the 30 orientations)

3.3 Hardware Selection

The selection of hardware for detecting defects in Mandarin Oranges, such as lenses, cameras, and industrial grade light sources, is determined by specific needs (Li *et al*., 2013).

1) The Mandarin Orange defect detection system benefits from the use of LED ball ring lights because of their high light intensity and compact size, making them the preferred lighting system and illumination approach. Position the industrial camera in the exact same spot as the light source and examine the vertical illumination of the light source from top to bottom. Simultaneously, change the aperture to the appropriate setting and secure it in place (Xu, Sun, & Ye, 2020).

2) In the machine vision system, the camera plays a crucial role in capturing and interpreting the reflected light from the object. The device turns light into analog signals and subsequently changes the analog signals into digital signals for transmission to other devices Manish, Venkatesh, & Ashok, 2018). The Hikvision industrial camera model MV-CU013-21UM is chosen due to its ability to satisfy the demands of visual analysis with its high speed and precision. The selected lens is the MVL-HF0828M-6MPE model, which features a focus mechanism. The image exhibits high clarity and excellent contrast, designed for a field of view measuring 203mm × 170mm. The lens's lower end has a minimum object distance of 200 mm, as determined by the chosen industrial camera. A resolution of 1.3 megapixels (1248 × 1024, with a pixel size of 4.8 μm × 4.8 μm) may attain an accuracy of 0.038 mm per pixel.

3.4 Software Selection

Image Advances in computer vision technology constantly upgrade and enhance image processing techniques and tools. The Halcon development environment provides a comprehensive visual processing library that includes a wide range of both basic and advanced image processing techniques. These techniques include everything from capturing pictures from different hardware devices to implementing complex pattern-matching algorithms. In addition, it provides several tools often utilized in machine vision applications, including tools for file processing, data analysis, algorithm operations, and classification (Luo *et al*., 2011). This study developed an image processing method utilizing the Halcon development environment to accurately detecting the size, color, and imperfections of oranges.

4. Orange grade classification Algorithms

This study uses image processing algorithms to identify the defect areas on Mandarin orange skin in the original image, as shown in Figure 3.

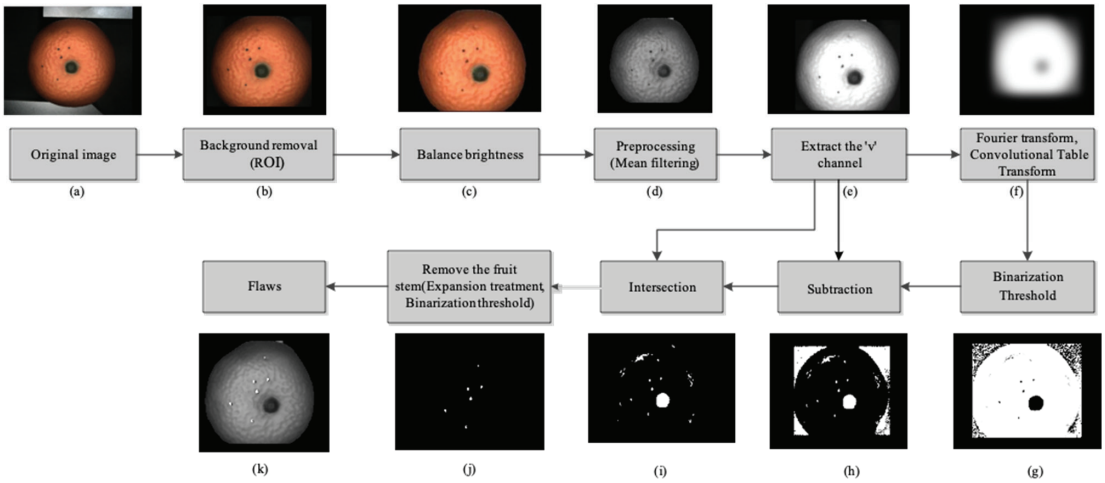

Figure 3. Procedure for identifying areas of defects on orange skin

4.1 Background Removal

Computer vision utilizes blob detection algorithms to locate sections in a digital image that display noticeable characteristics, such as differences in brightness or color, compared to the surrounding areas. Essentially, a blob refers to a distinct portion of an image that exhibits uniform or almost uniform attributes, resulting in all the pixels within it being similar to one another, as shown in Figure 3 (a).

There are three sequential steps in the Halcon to separate the Mandarin orange from the background:

1) Determine the appropriate threshold for selecting the region of interest, which involves converting the image to binary format. Examine the gray-scale histogram and adjust the threshold value within the 0 to 255 range (Bin & Lei, 2022). The equation (1) can be used to determine the gray-scale value of the color image. This calculation uses the thresholds T1 and T2, along with the coordinates I(x, y) (Li & Du, 2023). The empirical threshold value for an orange picture falls between the range of 60 to 255.

$$g(x,y) = \begin{cases} 1, T_1 \le I(x,y) \le T_2 \\ 0, \quad others \end{cases} \qquad (1)$$

where:

$I(x,y)$ is Intensity of the pixel at (x,y).

T_1, T_2 is Minimum and maximum threshold values.

$g(x,y)$ is Binary output (1 for blob, 0 otherwise).

2) The area of interest (ROI) is chosen and the algorithm uses connected component labeling with either 4-connectivity or 8-connectivity.

4-connectivity: A pixel is connected if it shares a side with another pixel.

(a) Original image (b) ROI mask (c) Isolated area

Figure 4. Blob analysis rendering

The labeled regions are the blobs, which are mathematically defined as sets of connected pixels, as depicted in Figure 4(b).

3) The varying colors on the edges indicate distinct areas of noise. Open the feature histogram and select "area" in the feature selection and code generation tab to filter out isolated areas (Ji *et al*., 2018), as shown in Figure 4 (c).

Determining the ratio of defects present on the entire surface is crucial for categorizing defects on the fruit's skin. When blobs are detected, various features is computed using geometric and statistical equations:

3.1) Area: The area of a blob is the number of pixels in the region as shown by Equation (2).

$$\text{Area} = \sum_{(x,y)\in R} 1 \tag{2}$$

where R is the region corresponding to the blob.

3.2) Centroid: The centroid (x_c, y_c) of a blob is calculated as:

$$x_c = \frac{\sum_{(x,y)\in R} x}{\text{Area}}, \quad y_c = \frac{\sum_{(x,y)\in R} y}{\text{Area}} \tag{3}$$

where

x_c, y_c are centroid coordinates of the blob.

x, y are coordinates of each pixel in the blob.

R is the set of pixels belonging to the blob region.

$Area$ is the total number of pixels in the blob, given by Equation (2).

The varying colors on the edges indicate distinct areas of noise (Ji *et al*., 2018), as shown in Figure 4(c).

4.2 Balance Brightness

In many cases, brightness adjustments are needed the brightness of the acquired images due to environmental factors. The division technique is employed in this design (Dworkin & Nye, 2006). If $I(x,y)$ is the input image and $B(x,y)$ is the estimated background brightness. The balanced image $I'(x,y)$ can be calculated by using Equation (4), and the result is shown in Figure 5.

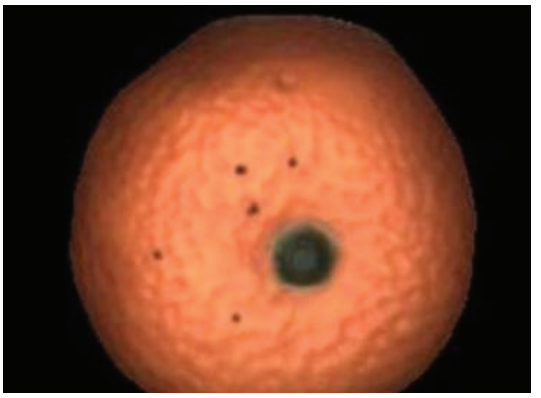

Figure 5. Illustrates the use of division to balance

$$I'_{(x,y)} = \frac{I_{(x,y)}}{B_{(x,y)}} \quad (4)$$

4.3 Preprocessing (Mean Filtering)

Image preprocessing is a fundamental step in image segmentation and feature extraction (Heena *et al*., 2020). The collected images are often affected by noise, so they must be pre-processed. An industrial camera captures a moment's worth of citrus photos on a roller. The usual filtering methods include Gaussian filtering, mean filtering, median filtering, and other methods (Lu & Li, 2024). This article adopts mean filtering. Mean filtering also belongs to a type of linear smoothing filtering, which is suitable for images that emphasize the overall pixel structure while ignoring detailed information (Othman *et al*., 2020). The principle of mean filtering is to use a scanning window to scan an image. When the window size is determined, the mean gray value of all pixels in the neighborhood of the pixel that coincides with the center of the window is taken as the gray value

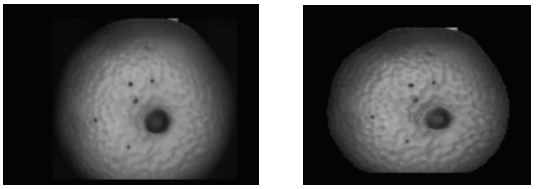

(a) Before filtering (b) After filtering

Figure 6. Compares the results before and after applying a filtering process

of that point (Zhao *et al*., 2016). Assuming $f(x,y)$ is a noisy picture and $g(x,y)$ is the filtered picture, the mathematical expression for the filtering result is Equation (5).

$$g(x,y) = \frac{1}{N} \sum_{(x,y)\in M} f(x,y) \quad (5)$$

This design utilizes a mean filter, and the Figure 6 displays a visual comparison of the average filtering effect.

4.4 Identifying Defects (Extract the "V" Channel)

After dividing the brightness balanced image into three channels, "R," "G," and "B," we observed that the red channel exhibited more prominent image defect characteristics. Consequently, we divided the image containing the red channel characteristics into "HSV," where "H" stands for hue, "S" for saturation, and "V" for brightness. The study observed that the "V" channel displayed flaws more clearly than the other two channels (Jolly & Raman, 2016), as illustrated in Figure 7.

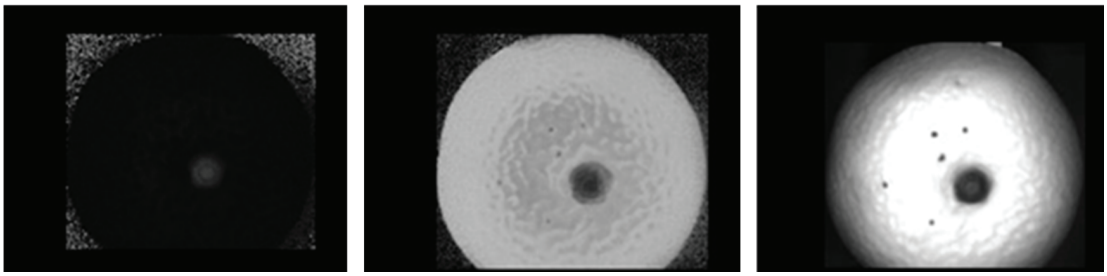

(a) H channel (b) S channel (c) V channel

Figure 7. "HSV" rendering

While the decomposition of the image itself does not directly involve complex mathematical equations, it can be described using the basic concept of how each color channel in an RGB image is extracted.

Each pixel point of the color image is decomposed into a red channel $I_R(x, y)$, a green channel $I_G(x, y)$, and a blue channel $I_B(x, y)$. The Equation (6) displays the specific formula.

$$Balance\ (x, y) = ((I_R(x, y), I_G(x, y), I_B(x, y)) \quad (6)$$

The equation of this operation can be expressed as the conversion of RGB to HSV color space. the Equations (7-9) of RGB to HSV conversion are:

Hue, $H(x, y)$:

$$H(x,y) = \begin{cases} 0 & (Condition\ 1) \\ 60° \times \frac{G(x,y) - B(x,y)}{\Delta}\ mod\ 360 & (Condition\ 2) \\ 60° \times \left(2 + \frac{B(x,y) - R(x,y)}{\Delta}\right) & (Condition\ 3) \\ 60° \times \left(4 + \frac{R(x,y) - G(x,y)}{\Delta}\right) & (Condition\ 4) \end{cases} \quad (7)$$

where

$$\text{Condition 1: } \Delta = 0;$$
$$\text{Condition 2: } I_R(x,y) = \max(I_R(x,y), I_G(x,y), I_B(x,y)),$$
$$\text{Condition 3: } I_G(x,y) = \max(I_R(x,y), I_G(x,y), I_B(x,y)),$$
$$\text{Condition 4: } I_B(x,y) = \max(I_R(x,y), I_G(x,y), I_B(x,y)),$$
$$\Delta = \max(I_R, I_G, I_B) - \min(I_R, I_G, I_B).$$

Saturation, $S(x, y)$:

$$S(x,y) = \begin{cases} 0 & Condition\ 1 \\ \frac{\Delta}{\max(I_R(x,y), I_G(x,y), I_B(x,y))} & Condition\ 2 \end{cases} \quad (8)$$

where

$$\text{condition 1: } \max(I_R(x,y), I_G(x,y), I_B(x,y)) = 0,$$
$$\text{condition 2: } \max(I_R(x,y), I_G(x,y), I_B(x,y)) > 0.$$

Value, $V(x, y)$:

$$V(x,y) = \max(I_R(x,y), I_G(x,y), I_B(x,y)) \quad (9)$$

The specialized formula for image subtraction utilized in the research encompasses the application of the "V" channel for definitive defect detection, subtraction for defect extraction, and the subtraction of three images corresponding to "R", "G", and "B".

Equation (10) delineates the operation that executes a pixel-by-pixel subtraction of the Blue () and Green () components.

$$Sub_{G(x,y)} = 20\big(B(x,y) - G(x,y)\big) - 200 \quad (10)$$

The equation yields an image difference. The obtained results can be employed to identify features in the image to generate an approximate defect map of Mandarin oranges, as illustrated in Figure 8.

4.5 Fourier Transform

Through Fourier transform, noise components in images, especially periodic noise, can be identified. Then, remove these noise components in the frequency domain to restore the image clearly. Fourier transform-based image denoising focuses on the separate frequency band information of the picture and noise to achieve image denoising (Ali & Pervaz, 2013). Typically, the high frequency spectrum distributes noise and edge information, while the low frequency range splits picture information.

The equation of Fourier transform is shown in Equation (11).

$$F(u,v) = \sum_{x=0}^{M-1}\sum_{y=0}^{N-1} f(x,y)e^{-j2\pi\left(\frac{ux}{M}+\frac{vx}{N}\right)} \quad (11)$$

where

x, y are time domain variables.

u, v are variables in the frequency domain.

M and N are the image's length and width.

$f(x, y)$ represents the two-dimensional plane image of row N and column M.

$f(u, v)$ is a Fourier transform.

Figure 9 shows Fourier transform effect after convolution.

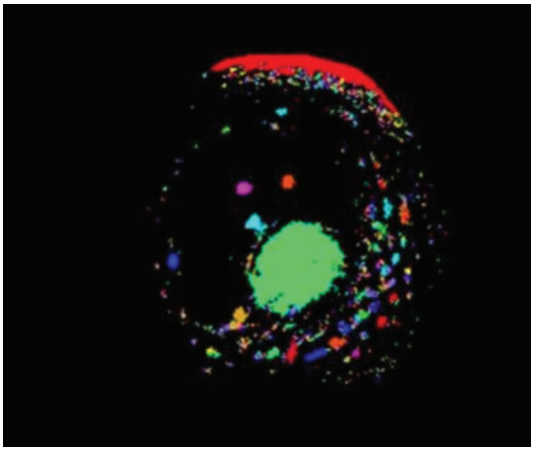

Figure 8. Rough defect effect

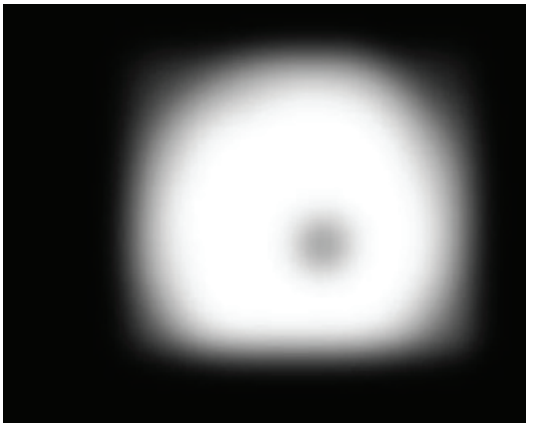

Figure 9. Convolutional effect of Fourier transform

4.6 Binarization Threshold

Binary thresholding is an image processing technique that converts grayscale images into images containing only two pixel values, typically black (0) and white (255), or other specified values. This process relies on selecting an appropriate threshold to classify pixel values into two categories.

The equation of Binary thresholding is

$$B(x,y) = \begin{cases} 255, & I(x,y) \geq T \\ 0, & I(x,y) < T \end{cases} \quad (11)$$

where

$I(x,y)$ is Intensity of the pixel at (x,y).

T is the threshold value.

$B(x,y)$ is Binary output (1 for blob, 0 otherwise).

Figure 10 displays the histogram of the binarization threshold obtained from an orange image.

4.7 Subtraction

The Subtraction is utilized to perform the subtraction of two images. The gray values of the removed image and the input image are denoted as g_1 and g_2, respectively, and will be transformed accordingly.

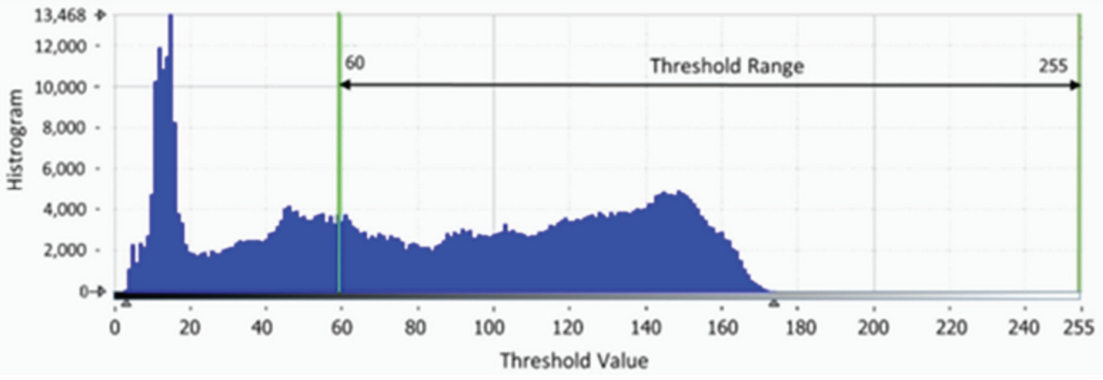

Figure 10. Binarization threshold histogram

Figure 11. Image after subtraction

$$g' = (g_1 - g_2) * Mult + Add \quad (12)$$

The image obtained after the subtraction process is shown in Figure 11.

4.8 Image Intersection

Image intersection refers to the set of pixel points or regions that are common to two image sets A and B, denoted as A ⋂ B. In the field of image processing, this usually means comparing the pixel data of two images on a point-by-point basis, to find the points or regions that are the same in terms of location and whose pixel values satisfy a specific condition (e.g., are equal or satisfy a certain relationship).

4.9 Removing Fruit Stems

Inflation, commonly referred to as the dilation of an image, is a mathematical procedure used to identify the local maximum value. Mathematically speaking, dilation or erosion can be defined as the convolution of picture A with kernel B. Determine the highest pixel value inside the coverage area of kernel B and apply this value to the pixel indicated by the reference point, thereby incrementally expanding the highlighted area in the image (Rahman *et al*., 2017).

Dilation in morphological operations can be represented mathematically as:

$$R'(x,y) = \max_{(u,v)\in S} R(x-u, y-v) \quad (13)$$

where

$R(x,y)$ is the input binary region (the set of pixels defining the region.

S is the structuring element, which is a circle in this case.

(u,v) is pixels in the structuring element.

$R'(x,y)$ is the output region after dilation.

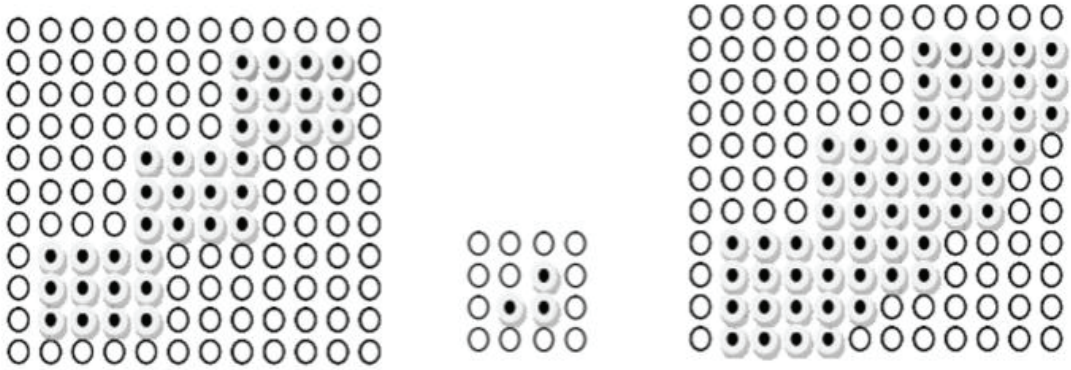

(a) Before Dilation (b) Structural element (C) After Dilation

Figure 12. Dilation schematic diagram (Chen, 2019)

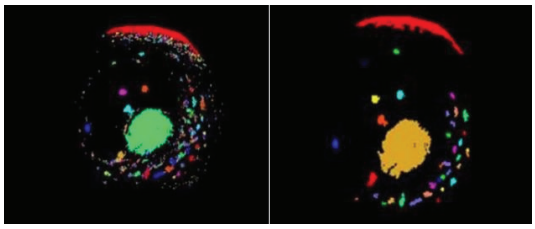

(a) Before image dilation (b) After image dilation

Figure 13. Comparison before and after dilation

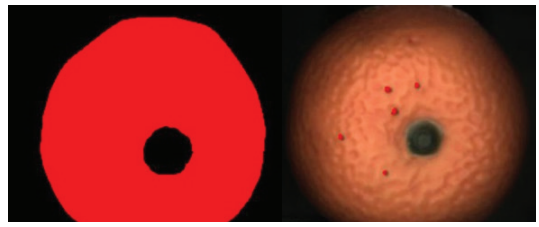

(a) (b)

Figure 14. Defect identification

Figure 12 shows the schematic diagram illustrating the process of dilatation, comparing the before and after states.

Figure 13 illustrates the contrast between the orange image's original and post-dilation version.

Finally, in order to generate an accurate map of fault locations, the process involves selecting relevant features, reducing the number of pictures, and removing fruit stems (Rong, Rao, & Ying, 2017), as shown in Figure 14 (a) and (b).

5. Results and Discussions

The primary aim of this article is to compare 30 photographs of each fruit using advanced image analysis techniques such as blob analysis, frequency domain analysis, image enhancement, and morphology. These techniques involve processes such as image noise reduction, image filtering, image segmentation, ROI extraction, Fourier transform, and a combination of subtraction and addition.

The main goal is to extract any defects present in the fruit. The Mandarin orange's quality level is calculated by selecting the highest value from an array that includes the defect results obtained from examining 30 photographs of each Mandarin orange.

Figure 15 displays the "values" which indicate the outcomes of defect identification for each of the 30 images obtained from a Mandarin Orange fruit. The "Max" represents the final result, which is the worst-quality image among the identified Mandarin Orange photos. Figure 16 shows the results of 4 types of orange classification that were captured from developed software. The designation '0' is used to denote fruits of special grade, whereas the designation "1" is used for first-level fruits, "2" for secondary fruits, and "3" for third-level fruits. Figure 16 also depicts the distinct flaws observed in various orange grades.

RadiusMax	30.5728
value2	[0, 0, 0, 0, 42, 0, 0, 0, 0, 0, 0, 0, 0, 0, 11, 0, 0, 0, 0, 32, 0, 0, 0, 0, 0, 0, 0, 37, 14]
eab_rectangle_Max	42
result	2
values	[2, 2, 2, 2, 2, 1, 0, 0, 0, 2, 2, 2, 2, 2, 2, 2, 0, 0, 0, 1, 1, 2, 2, 2, 0, 0, 0, 0, 0, 2]
Max	2

Figure 15. Output results

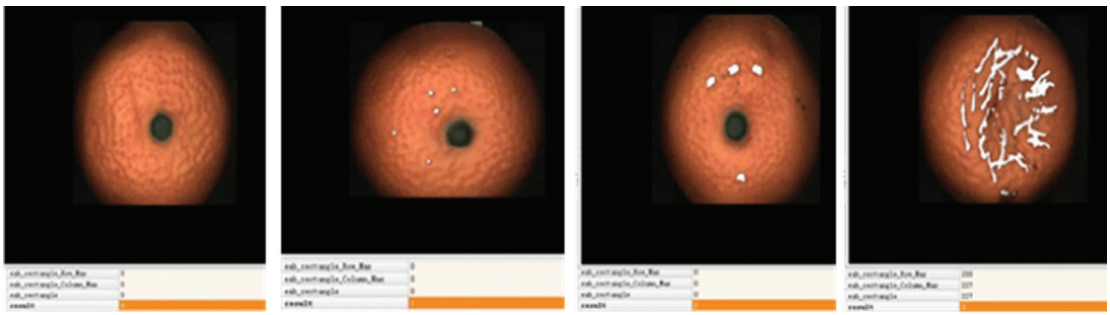

(a) Special Grade (b) Grade 1 (c) Grade 2 (d) Grade 3

Figure 16. Defect identification grade results from software

Defects on mandarin oranges is quite intricate, as indicated by the test results. However, the algorithm is able to accurately detect and categorize mandarin oranges with blemishes into four categories according to the specified requirements, as long as they fall within the algorithm's acceptable range. Table 2 shows the four varieties of mandarin oranges available on the market that meet the testing criteria. Using the calibrated scale of the camera, it has been determined that the length of 1 pixel is 0.038 mm. To clarify, a measurement of 1 mm. is approximately equivalent to 26 pixels.

This experimental method will greatly improve the efficiency compared to manual detection, but although it can accurately detect the size of defects, the long time required for the roller to flip and collect 30 photos will reduce work efficiency. The actual production process can reduce the number of photos collected. And in complex and highly variable datasets, this method is not particularly effective. It can be combined with deep learning algorithms for analysis, which can quickly improve detection efficiency and accuracy of defect levels.

6. Conclusion

This article outlines the process for categorizing the quality of Mandarin oranges using a machine vision system. The system consists of a hardware and software component. The gear was specifically engineered to snap thirty images of the orange peel from various perspectives,

Table 2. Comparative analysis of experimental and validation results

No	Grade	Variable	Standard size of defect		Measured defect size	
			pixel	mm.	pixel	mm.
1	Special grade	Circular_diameter_max	0	0	0.00	0.00
		Rectangle_max	0	0	0.00	0.00
2	Grade 1	Circular_diameter_max	> 0 to 40	> 0 to 1.52	30.08	1.14
		Rectangle_max	> 0 to 40	> 0 to 1.52	53.16	2.02
3	Grade 2	Circular_diameter_max	> 40 to 180	> 1.52 to 6.84	60.14	2.29
		Rectangle_max	≤ 40	≤ 1.52	39.00	1.48
		or				
		Circular_diameter_max	≤ 40	≤ 1.52	19.20	0.73
		Rectangle_max	> 40 to 180	> 1.52 to 6.84	176.6	6.71
4	Grade 3	Circular_diameter_max	> 180	> 6.84	140.30	5.33
		Defect area/	> 10%	> 10%	31,268.10	12.68%
		The total area			246,527.38	
		or				
		Rectangle_max	>180	> 6.84	242.00	9.19
		Defect area/	> 10%	> 10%	33,619.00	10.08%
		The total area			333,223.00	

while the software was specifically programmed to categorize different classes of oranges based on the sizes of imperfections on the peel. The fault can be identified by employing diverse image processing methods, such as picture capture, blob analysis, pre-processing, segmentation, feature extraction, morphology, median filtering, and the Fourier transformed. The faulty pixels were measured for their diameter and area in order to classify them for grading, as presented in Table 2.

Through the preliminary experiments and the results shown in Table 2 above, it can be learned that the image processing system in the Vaugan sorting system can operate normally and can meet the basic sorting requirements.

After the initial experiment in Table 2, it can be found that this system has a certain degree of accuracy for the recognition of mandarin oranges, but the recognition of the number of experiments need to be many times in order to obtain more accurate results, the next in a batch of mandarin oranges in the selection of 40, 10 mandarin oranges of each grade, after repeated experiments can be obtained after the experimental results of the following Table 3.

Table 3. Statistics of the results of multiple experiments on the same batch

	Special grade	Grade 1	Grade 2	Grade 3
Number of experiments (number)	10	10	10	10
Number of correct discriminations (number)	9	8	9	9
Number of misjudgments (number)	1	2	1	1
Accuracy rate	**90%**	**80%**	**90%**	**90%**

Through the experiment, we can find that the recognition accuracy of this system because we do not do deep machine learning at the same time for the characteristics of image processing, the judgment does not contain a variety of fruits on the market, so after a number of experiments with the same batch of mandarin oranges, this system for the experimental batch of mandarin oranges for the recognition of 90% accuracy of the special fruit, for the recognition of the first-class fruits of the accuracy of 80%, for the recognition of the second class of fruits of the accuracy of 90%, three class of fruits of the recognition accuracy of 90%, the overall actual recognition accuracy of 87 5%. The overall recognition accuracy of the system is 87.5%, which is 90% for first-grade fruits, 90% for second-grade fruits, and 90% for third-grade fruits.

The system has a certain number of misjudgments for the analysis of the fruit, and the system can be improved from the following two aspects in response to the situation:

1) Optimization of the visual algorithm part as well as deep learning, with different batches of different origins of mandarin oranges for experiments, and more epidermal disease eigenvalue judgments, at the same time, according to the different special circumstances of the miscarriage of justice so that the visual system for deep learning, reduce the miscarriage of justice rate.

2) This system sorts the knowledge of mandarin oranges purely through the epidermis of mandarin oranges for sorting, but in practice, part of the mandarin oranges are good or bad also need to be analyzed from the inside of the mandarin oranges, so in the practical application, only for the epidermis of the sorting of the precise may have errors, so it is necessary to combine with the corresponding technology to identify the inside of the comprehensive analysis so as to go to the precise sorting

Acknowledgments

The authors express their gratitude to Guilin University of Technology, China, for the financial support granted, including project numbers 2023B52 and 2022530A. We would like to express our gratitude to the Faculty of Engineering, Mahasarakham University, Thailand, for their support of facilities.

References

Ali, S. R., & Pervaz, S. (2013). Use of Fourier transformations and wavelets for satellite image processing. *2013 International Conference on Aerospace Science & Engineering (ICASE)*, 1–6. https://doi.org/10.1109/icase.2013.6785559

Batuman, O., Ritenour, M., Vicent, A., Li, H., Hyun, J.-W., Catara, V., Ma, H., & Cano, L. M. (2020). Diseases caused by fungi and oomycetes. *The Genus Citrus*, 349–369. https://doi.org/10.1016/b978-0-12-812163-4.00017-6

Behera, S. K., Jena, L., Rath, A. K., & Sethy, P. K. (2018). Disease classification and grading of orange using machine learning and fuzzy logic. *2018 International Conference on Communication and Signal Processing (ICCSP)*, 0678–0682. https://doi.org/10.1109/iccsp.2018.8524415

Bin, Z., & Lei, H. (2022). research on the drum brake surface defect detection based on HALCON. *2022 IEEE 5th Advanced Information Management, Communicates, Electronic and Automation Control Conference (IMCEC)*, 1452–1456. https://doi.org/10.1109/imcec55388.2022.10019807

Chen, S. (2019). *Design and implementation of surface defect detection algorithm for unfixed shading sanitary product* [Master's thesis]. Chinese Master's Theses Full-text Database. https://kns.cnki.net/KCMS/detail/detail.aspx?dbname=CMFD201901&filename=1019013553.nh

Chen, Y., Wu, J., & Cui, M. (2018). Automatic classification and detection of oranges based on computer vision. *2018 IEEE 4th International Conference on Computer and Communications (ICCC)*, 1551–1556. https://doi.org/10.1109/compcomm.2018.8780680

Dey, A., Biswas, S., & Le, D.-N. (2023). Recognition of human interactions in still images using AdaptiveDRNet with multi-level attention. *International Journal of Advanced Computer Science and Applications, 14*(10). https://doi.org/10.14569/ijacsa.2023.01410103

Dharmasiri, S. B. D. H., & Jayalal, S. (2019). Passion fruit disease detection using image processing. *2019 International Research Conference on Smart Computing and Systems Engineering (SCSE)*, 126–133. https://doi.org/10.23919/scse.2019.8842799

Dheeraj, H. P., Prabhu, A., Rani, N. S., & Jeevan, B. (2023). Deep learning models for classification of okra fruit diseases. *2023 3rd Asian Conference on Innovation in Technology (ASIANCON)*, 1–6. https://doi.org/10.1109/asiancon58793.2023.10270241

Dworkin, S. B., & Nye, T. J. (2006). Image processing for machine vision measurement of hot formed parts. *Journal of Materials Processing Technology, 174*(1–3), 1–6. https://doi.org/10.1016/j.jmatprotec.2004.10.019

Garg, N., Gupta, R., Kaur, M., Ahmed, S., & Shankar, H. (2023). Efficient Detection and Classification of Orange Diseases using Hybrid CNN-SVM Model. *2023 International Conference on Disruptive Technologies (ICDT)*, 721–726. https://doi.org/10.1109/icdt57929.2023.10150721

GB/T 40752-2021. (2021). *Specifications for operation management of orah poverty alleviation project(s)*. Retrieved November 25, 2021, from http://my678.cn/download-p254314.html

Hafiz, R., & Fatema, K. (2023). Wax apple disease detection and curative solution recommendation system using machine learning. *2023 14th International Conference on Computing Communication and Networking Technologies (ICCCNT)*, 1–6. https://doi.org/10.1109/icccnt56998.2023.10307412

Heena, A., Biradar, N., Maroof, N. M., & P, V. (2022). Processing of echocardiographic images using segmentation, feature extraction and classification for detection of heart abnormality. *Global Transitions Proceedings, 3*(1), 13–19. https://doi.org/10.1016/j.gltp.2022.04.003

Huang, T., Zheng, B., Zhang, J., Yi, C., Jiang, Y., Shui, Q., & Jian, H. (2021). Mango surface defect detection based on HALCON. *2021 IEEE 5th Advanced Information Technology, Electronic and Automation Control Conference (IAEAC)*, 2627–2631. https://doi.org/10.1109/iaeac50856.2021.9390783

Ji, Y., Zhao, Q., Bi, S., & Shen, T. (2018). Apple color automatic grading method based on machine vision. *2018 Chinese Control and Decision Conference (CCDC)*, 5671–5675. https://doi.org/10.1109/ccdc.2018.8408121

Jolly, P., & Raman, S. (2016). analyzing surface defects in apples using Gabor features. *2016 12th International Conference on Signal-Image Technology & Internet-Based Systems (SITIS)*, 178–185. https://doi.org/10.1109/sitis.2016.36

Kamalakannan, A., & Rajamanickam, G. (2012). Surface defect detection and classification in mandarin fruits using fuzzy image thresholding, binary wavelet transform and linear classifier model. *2012 Fourth International Conference on Advanced Computing (ICoAC)*, 1–6. https://doi.org/10.1109/icoac.2012.6416829

Li, D., & Du, F. (2023). Design of circulating commodity garbage classification system based on machine vision. *2023 IEEE 6th International Conference on Information Systems and Computer Aided Education (ICISCAE)*, 123–127. https://doi.org/10.1109/iciscae59047.2023.10393127

Li, J., Rao, X., Wang, F., Wu, W., & Ying, Y. (2013). Automatic detection of common surface defects on oranges using combined lighting transform and image ratio methods. *Postharvest Biology and Technology, 82*, 59–69. https://doi.org/10.1016/j.postharvbio.2013.02.016

Lu, G., & Li, K. (2024). Smoothing denoising method of spatial filtering image based on Contourlet transform. *Journal of Radiation Research and Applied Sciences, 17*(1), 100803. https://doi.org/10.1016/j.jrras.2023.100803

Luo, H., Long, Y., Xie, X.-B., & Huang, J.-C. (2011). Realization of vehicle license plate character recognition based on HALCON. *2011 4th International Congress on Image and Signal Processing*, 936–939. https://doi.org/10.1109/cisp.2011.6100314

Manish, R., Venkatesh, A., & Ashok, S. D. (2018). Machine vision based image processing techniques for surface finish and defect inspection in a grinding process. *Materials Today: Proceedings, 5*(5), 12792–12802. https://doi.org/10.1016/j.matpr.2018.02.263

Mojumdar, M. U., & Chakraborty, N. R. (2021). Orange & orange leaves diseases detection using computerized techniques. *2021 12th International Conference on Computing Communication and Networking Technologies (ICCCNT)*, 1–4. https://doi.org/10.1109/icccnt51525.2021.9579964

Othman, P. Sh., Marqas, R. B., Abdulqader, D. N., & Almufti, S. M. (2020). Effect of mean filter on face image from video frames. *2020 8th International Symposium on Digital Forensics and Security (ISDFS)*, 1–7. https://doi.org/10.1109/isdfs49300.2020.9116277

Prabhu, A., Likhitha, S., & Sangeetha, K. V. (2021). Identification of citrus fruit defect using computer vision system. *2021 Second International Conference on Electronics and Sustainable Communication Systems (ICESC)*, 1264–1270. https://doi.org/10.1109/icesc51422.2021.9532834

Rahman, A. N., Heriana, O., Putranto, P., Darwis, F., Pristianto, E. J., & Wijayanto, Y. N. (2017). Morphological dilation for radar image enhancement. *2017 International Conference on Radar, Antenna, Microwave, Electronics, and Telecommunications (ICRAMET)*, 68–71. https://doi.org/10.1109/icramet.2017.8253147

Rong, D., Rao, X., & Ying, Y. (2017). Computer vision detection of surface defect on oranges by means of a sliding comparison window local segmentation algorithm. *Computers and Electronics in Agriculture, 137*, 59–68. https://doi.org/10.1016/j.compag.2017.02.027

Sangkatip, W., Chomphuwiset, P., Bunluewong, K., Mekruksavanich, S., Okafor, E., & Surinta, O. (2024). Improving neural network-based multi-label classification with pattern loss penalties. *IEEE Access, 12*, 52237–52248. https://doi.org/10.1109/access.2024.3386841

Spreen, T. H., Gao, Z., Fernandes, W., & Zansler, M. L. (2020). Global economics and marketing of citrus products. *The Genus Citrus*, 471–493. https://doi.org/10.1016/b978-0-12-812163-4.00023-1

Xu, L., Sun, H., & Ye, X. (2020). Nondestructive testing method for surface defects of mechanical parts based on machine vision. *2020 International Conference on Robots & Intelligent System (ICRIS)*, 92–95. https://doi.org/10.1109/icris52159.2020.00031

Zhao, J., Xia, X., Wang, H., & Kong, S. (2016). Design of real-time steel bars recognition system based on machine vision. *2016 8th International Conference on Intelligent Human-Machine Systems and Cybernetics (IHMSC)*, 505–509. https://doi.org/10.1109/ihmsc.2016.75